

Ultra-high frequency magnetic resonance through strain-spin coupling in perpendicular magnetic multilayers

De-Lin Zhang^{1†}, Jie Zhu^{2†§}, Tao Qu^{3†}, Dustin M. Lattery^{2†}, R. H. Victora^{1,3*}, Xiaojia Wang^{1,2*} and Jian-Ping Wang^{1*}

1. Department of Electrical and Computer Engineering, University of Minnesota, MN 55455, USA;
2. Department of Mechanical Engineering, University of Minnesota, MN 55455, USA;
3. School of Physics and Astronomy, University of Minnesota, MN 55455, USA;

[†]These authors have equal contributions to this work.

[§]Present address: Key Laboratory of Ocean Energy Utilization and Energy Conservation of Ministry of Education, Dalian University of Technology, Dalian, Liaoning 116024, China.

*Author to whom correspondence should be addressed: jpwang@umn.edu, wang4940@umn.edu and victora@umn.edu

The interaction between strain and spin has received intensive attention in the scientific community due to its abundant physical phenomena and huge technological impact. Until now, there is no experimental report on ultra-high frequency magnetic resonance through the strain-spin coupling for any technologically relevant perpendicular magnetic material. Here we report the experimental detection of the acoustic strain waves that have a response time on the order of 10 picoseconds in perpendicular magnetic [Co/Pd]_n multilayers via a femtosecond laser pulse excitation. Through direct measurements of acoustic strain waves, we observe an ultra-high frequency magnetic resonance up to 60 GHz in [Co/Pd]_n multilayers. We further report a theoretical model of the strain-spin interaction. Our model reveals that the energy could be transferred efficiently from the strain to the spins and well explains the existence of a steady resonance state through exciting the spin system. The physical origins of the resonance between strain waves and magnetic precession, and the requested conditions for obtaining magnetic resonance within thin magnetic films have also been discussed after thorough analysis. These combined results point out a potential pathway to enable an extremely high frequency (EHF) magnetic resonance through the strain-spin coupling.

Exploring innovative approaches and new physics to manipulate the magnetization of ferromagnetic materials via femtosecond laser pulses has recently renewed interests in both scientific and technological communities¹⁻³. The coupling between strain and spin has received intensive attention in the scientific community due to its abundant physical phenomena⁴⁻¹¹. Meanwhile, experimentally utilizing femtosecond lasers to manipulate the magnetic properties of materials with perpendicular magnetic anisotropy (PMA) through the coupling between strain and spin has become a promising area for developing ultralow-energy spin memory and logic devices¹²⁻¹⁶.

To date, the main efforts have been devoted to strain generated from piezoelectric materials¹⁷⁻²⁰ *via* electrical methods. It was first discovered by Beaurepaire *et al.* in 1996 that femtosecond laser pulses can modify the magnetization of ferromagnetic materials through thermally induced demagnetization²¹. This ultrafast optical approach provides a powerful tool for capturing the energy-carrier interactions between electrons, spins, and phonons in the femtosecond time regime²²⁻²⁷. Through the magnetostriction effect of ferromagnetic (FM) materials, acoustic strain waves (ASWs) can be launched by femtosecond laser pulses^{13,28-35}. Upon femtosecond laser pulse excitation, ASWs directly act through the entire FM film and thus can readily couple with the spins to modify the magnetic anisotropy and, subsequently, magnetization of a FM material. In addition, its picosecond time scale corresponds to the time scale of the magnetization precession and has potential to stimulate abundant physical phenomena, such as large-angle rotation/precession. Specifically, this strain can couple with spins through a magnon-phonon interaction to induce the magnetic resonance and even further switch magnetization with a large angle magnetization precession through high resonance frequency¹³.

Motivated by this idea, many experimental and theoretical studies have reported the magnetization dynamics of ferromagnetic thin films under optically generated ASWs. However, the materials studied so far have not been applicable to spintronic applications due to low magnetic moment, low anisotropy, or low Curie temperature, such as dilute semiconductor materials^{28,29,31,33,34} and metallic FM materials (*e.g.*,

Terfenol-D ((Tb_xDy_{1-x})Fe₂)¹³, Galfenol^{32,35}, Bi-YIG³⁶ and Ni³⁰). As a matter of fact, direct experimental demonstration of the coupling between ASWs and spins in PMA materials remains elusive, despite the fundamental importance of the physical mechanisms of magnetic resonance. [Co/Pd]_n multilayers possess high PMA at room temperature, holding great potential for various technological applications³⁷⁻⁴¹. Furthermore, [Co/Pd]_n multilayers have a relatively large magnetostriction coefficient λ ($\sim -1 \times 10^{-4}$)^{42,43}, thus their acoustic frequency can be easily tuned by varying the film thickness. This could serve as an ideal platform for investigating the magnetic resonance.

Here we experimentally report an ultra-high frequency magnetic resonance up to 60 GHz in perpendicular magnetic [Co/Pd]_n multilayers through the strain-spin coupling excited by femtosecond laser pulses. Differentiating from the anti-crossing behavior (incoherent magnon ($\mathbf{k} \neq 0$)-phonon ($\mathbf{q} \neq 0$) interaction) in ferromagnetic insulators¹⁰, we observe a crossing intersection in the energy for coherent magnon ($\mathbf{k} = 0$)-phonon ($\mathbf{q} = 0$) interaction in PMA [Co/Pd]_n multilayer materials. Meanwhile, the ASWs are experimentally detected via the time-domain thermoreflectance (TDTR) method on the order of 10 picoseconds. We also theoretically investigate that ASWs can manipulate the magnetization and could further assist the switching in an ultrafast picosecond scale. These combined results pave a potential pathway to enable an extremely high frequency (EHF) magnetic resonance through the strain-spin coupling and suggest a possibility of ultrahigh-speed strain-assisted magnetization switching in a technologically relevant magnetic system.

Results

Ultrafast measurement protocol. Figure 1a illustrates the time-resolved magneto-optical Kerr effect (TR-MOKE) measurement configuration together with a schematic of the sample stack. The phonon temperature⁴⁴ and strain from thermoreflectance signals⁴⁵ collected in time-domain thermoreflectance (TDTR) measurements are proportional to the intensity change in the reflectivity of the probe beam. Thus, the TDTR signals measured here represent the intrinsic strain waves in the sample. The

TR-MOKE method employed here is a pump-probe technique capable of recording the time evolution of magnetization (\mathbf{M}), through the change in the polarization of a probe beam reflected from FM films. For a typical polar TR-MOKE measurement, a damped oscillation feature is expected in the signals due to the spin precession initiated by the rapid temperature rise from pump excitation, when an external magnetic field (H_{ext}) is applied⁴⁴. In Supplementary Note 1, more details about the TDTR and TR-MOKE experiment setups and signal detection methods can be found. The signals from TR-MOKE measurements contain information of two modes, as the superposition of two frequencies in M_z : the field-dependent one corresponding to the typical ferromagnetic resonance resulting from coherent spin precession (the spin-like mode), and the field-independent one caused by a time-dependent modulation of magnetic properties through strain (the strain-like mode). We provide more detailed definitions and physical origins of the two oscillation modes in Supplementary Note 2. The simulated spin dynamic processes in the TR-MOKE measurements in or out of resonance are illustrated by Supplementary Figs. 5 and 6, respectively. When the sample has a large λ , ASWs can also tilt the magnetization and therefore create a detectable change in M_z and will be captured as magnetization oscillations in the signal as well. Thus the magnetization oscillation features captured by TR-MOKE contains both the spin precession and ASWs information. Therefore, analysing the data from both TDTR and TR-MOKE measurements allows for the investigation of the coupling between strain and spin.

In typical polar TR-MOKE measurements, signals usually do not show magnetization oscillations in the absence of H_{ext} , since the equilibrium axis of the spin precession will be aligned with the surface normal direction of the perpendicular magnetic film. In our TR-MOKE signals for all the $[\text{Co/Pd}]_n$ samples, the magnetization oscillations appear as a function of time without H_{ext} , implying that these samples possess the magnetostriction effect, as discussed in the Supplementary Note 1 and shown in Supplementary Figs. 1 and 2. This phenomenon is not observed in the $[\text{Co/Pt}]_n$ sample (not shown here) due to its relatively small magnetostriction coefficient⁴². By

fitting the TR-MOKE data, we found that in relatively thin films, the strain frequency (> 100 GHz) is much higher than that of spin precession (< 60 GHz) with a relatively low H_{ext} , as shown in Supplementary Fig. 3. This frequency is for the lowest-frequency mode of the standing strain waves confined within the thin-film sample stack, whose half wavelength corresponds to the thickness of the entire sample stack (including the capping and seed layers). Therefore, by changing the sample thickness, the strain frequency can be tuned⁴⁵. In this study, we select the [Co(0.8 nm)/Pd(1.5 nm)]₁₁ multilayered structure with a larger thickness as a model system. This [Co(0.8 nm)/Pd(1.5 nm)]₁₁ multilayer is seeded with a Ta(5 nm)/Pd(5 nm) bilayer deposited on a SiO₂ (300 nm)/Si substrate and is capped with a 3-nm Ta layer. It has perpendicular anisotropy with an effective field of $H_{k,\text{eff}} \sim 6.5$ kOe and magnetic anisotropy of $K_u \sim 4.4$ Merg/cc, as shown in Fig. 1b.

Ultrafast measurement results. The TR-MOKE results of [Co(0.8 nm)/Pd(1.5 nm)]₁₁ with the range of H_{ext} from 10 kOe to 29 kOe are plotted in Fig. 2a. Interestingly, we find that for $16 \text{ kOe} < H_{\text{ext}} < 25 \text{ kOe}$, TR-MOKE signals show the amplitude of precessional oscillations of M_z increase instead of the usual decrease in the first 60 ps following the pump excitation. However, when H_{ext} is smaller than 16 kOe or larger than 25 kOe, the TR-MOKE signals in Fig. 2a appear as the damped oscillations (standard in TR-MOKE measurements of magnetization precession). Within the first several picoseconds, different energy carriers such as magnons, phonons, and electrons are out of equilibrium with each other induced by the ultrafast laser pulse. As the main goal of this work is to analyze the magnetic precession that is in the equilibrium regime, we purposefully start the fitting from 10 ps to avoid any possible non-equilibrium effect (indicated by the solid lines in Fig. 2a). From Fig. 2b of TDTR data, we can find that the acoustic strains prevail in the first 60 ps, suggesting the magnetic resonance increases the energy transferred from ASWs to spin precession within the first 60 ps. As this injected energy overcomes the dissipated energy, the amplitude of spin precession is enhanced, in contrary to the monotonic decaying trend of a typical damped feature of spin precession at other fields. After 60 ps, the injected energy by the strain

is insufficient to equilibrate the dissipated energy due to the damping, thus not capable to maintain the high energy state (resonance state). The spin oscillation amplitude decreases, and the typical damped feature appears. This phenomenon indicates that during this first 60-ps time regime, the magnetostrictive field generated by ASWs couples with spins and further enhances the spin precession.

To further understand the magnetization dynamics and magnetic resonance resulting from the coupling between strain and spin, the TR-MOKE and TDTR signals of the [Co(0.8 nm)/Pd(1.5 nm)]₁₁ sample are analyzed in the time domain using the following equation:

$$V(t) = A + Be^{-t/C} + D_1 \sin(2\pi f_1 t + \varphi_1) e^{-t/\tau_1} + D_2 \sin(2\pi f_2 t + \varphi_2) e^{-t/\tau_2}, \quad (1)$$

where V is the signal, t is the time, A , B , and C are fitting parameters of the thermal background, D_i represents the amplitude of sinusoid, f_i is the frequency, and τ_i is the relaxation frequency (where $i = 1, 2$ represents separate modes captured by the measurement simultaneously)^{41,42,46-49}. The TDTR data only show one frequency corresponding to the picosecond acoustics (strain) in the system, which is independent of the external field. Fitting the TR-MOKE data (which captures the change in the z -component of magnetization) shows two frequencies: a frequency that depends on H_{ext} following a Kittel dispersion (assigned as the “spin-like” mode), and a frequency that is independent of H_{ext} that matches the frequency of the strain captured by TDTR (assigned as the “strain-like” mode). The amplitude and phase information of the modes (φ_i) can also differentiate the two modes (see Supplementary Note 1). Two TR-MOKE signals, one in resonance ($H_{\text{ext}} = 21$ kOe) and the other one out of magnetic resonance ($H_{\text{ext}} = 14$ kOe), are chosen to study the coupling between spin precession and ASWs based on Eq. (1). We find that the frequency of the signal without the magnetic resonance shows two separated peaks, ~ 38 GHz for spin precession and ~ 60 GHz for ASWs, as shown in Fig. 2c. However, for the signal with the magnetic resonance, two frequency peaks are overlapping at ~ 60 GHz, as plotted in Fig. 2d. This suggests that the magnetic resonance originates from the strong coupling between strain and spin.

Ultra-high frequency magnetic resonance. The frequencies of spin precession of the [Co(0.8 nm)/Pd(1.5 nm)]₁₁ multilayer are fitted from the TR-MOKE signal as a function of H_{ext} using Eq. (1), and the results are plotted in Fig. 3a. The frequencies obtained from the TR-MOKE signals are respectively assigned to the strain-like mode (red diamonds) and spin-like mode (black circles). It is found that the frequency of the strain-like mode remains constant at ~ 60 GHz, which is almost the same value as the frequency (blue stars) of ASWs fitted from the TDTR signals. The frequency of the spin-like mode shows a linear behavior as a function of H_{ext} . The frequency value increases from ~ 15 GHz to 80 GHz and crosses the ASWs frequency at $H_{\text{ext}} \approx 21$ kOe (mode-crossing field). Magnetic resonance is observed around this mode-crossing field, indicating that with close or comparable frequency, ASWs can significantly influence the spin dynamics and induce magnetic resonance. Normally, the incoherent magnon ($\mathbf{k} \neq 0$)-phonon ($\mathbf{q} \neq 0$) interactions in ferromagnetic insulators couple with an anti-crossing point in the dispersion, where the magnon and phonon frequencies do not show mode crossing with H_{ext} , instead splitting and opening up gaps at dispersion intersecting points of the spin wave and acoustic phonon¹⁰. Instead, we observe a crossing intersection in the dispersion of coherent modes. For the amplitude of M_z (proportional to terms D_1 and D_2 in Eq. (1)) shown in Fig. 3b, we distinguish the two modes by considering the modes that have a constant frequency to be strain-like. From Fig. 3b, we find the amplitude of M_z shows resonant behavior; the amplitude of M_z associated with the strain-like mode keeps constant and increases around the mode-crossing field, and that of the spin-like mode follows the same trend around the mode-crossing field. This suggests that if the frequency is similar, strain strongly couples with spins and enhances the amplitude of magnetization precession, presenting the mode mixing characteristic of the magnon-phonon coupling in the [Co(0.8 nm)/Pd(1.5 nm)]₁₁ multilayer. Importantly, because this resonance field depends on the ASW frequency and Kittel dispersion, the tunability of the resonance field can be verified by tuning the sample thickness and magnetic anisotropy (see Supplementary Note 3 and Supplementary Table 1, Figs.7 and 8). In order to accurately model the magnetization

dynamics in the system with micromagnetic simulations, we analyze the TR-MOKE signal and obtain a precessional cone angle ~ 1 degree through a straightforward voltage to Kerr angle conversion. This cone angle is important to determine the correct initial condition for the magnetization (see Supplementary Note 4).

To suggest material and system properties capable of exhibiting a magnetic resonance, and to provide physical insights into the experimental results, a micromagnetic simulation based on the Landau-Lifshitz-Gilbert (LLG) equation is employed. A physical model to describe the interaction between magnon ($\mathbf{k} = 0$) and phonon ($\mathbf{q} = 0$) is implemented through the introduction of a magnetostrictive energy. The magnetostrictive energy functions as a temporal effective perpendicular anisotropy in our $[\text{Co/Pd}]_n$ multilayers along the specific $[111]$ orientation. The effective anisotropy has an oscillatory behavior with the frequency determined by the strain, proved in Supplementary Note 6A. The minimum point of the magnetostrictive energy is alternating between out-of-plane (when the thin film undergoing compression) and in-plane (inversely, expansion). The magnetostrictive energy is comparable with the energy barrier of the pure magnetic system, as the perpendicular anisotropy cancels the demagnetization effect. Before we carry out the simulations, the strain amplitude is optimized. As the energy simulation results show, when the strain amplitude is 0.1% at the beginning 100 ps, the pumped energy dominates and wins over the dissipated energy. Thus the spin system can be excited to a non-equilibrium state. This energy pumping is efficient, as the excited state is achieved in less than hundreds of picoseconds. This excited state represents the magnetic resonance and can be maintained if a way to produce stable ASWs is applied (see Supplementary Note 6C and Supplementary Fig. 9). For a realistic strain as 0.1% estimated from experimental data, the amplitude of the magnetostrictive anisotropy is $3.9 \times 10^4 \text{ erg/cm}^3$, a significant change in anisotropy when compared with the effective PMA of $9.2 \times 10^5 \text{ erg/cm}^3$. Considering the spin system is essentially a nonlinear system, the magnetostrictive anisotropy as a driving field can efficiently excite the spins from their equilibrium state and achieve a large oscillation amplitude. This large oscillation shows a circular polarization,

differentiating from linear polarization of in-plane materials, as discussed in Supplemental Note 2. The strain-like and spin-like modes entangle and cause frequency beating at off-resonance points. These two modes resonate when their frequencies match. The spins precess into a larger oscillation when the energy pumped from strain enhances the system total energy level, overcoming the dissipated energy caused by the damping effect. The theoretical rising time is influenced by the strain amplitude and the angle of H_{ext} in Eq. (S30) of Supplementary Note 6C. The simulated rising time in Fig. 4b reproduces the TR-MOKE signal in Fig. 4a without using fitting parameters for the materials. This confirms the accuracy of our theory. The spins behave damped when the strain decays because the pumped energy, as proportional to the strain, is not sufficient to compensate the dissipated energy. The oscillation amplitude of M_z as a function of H_{ext} shows a peak around the mode-crossing field, and its intensity increases with the increase of the strain, which well matches the experimental results shown in Fig. 3b.

Time-dependent magnetization dynamics driven by ASWs. To prove ASWs can manipulate the magnetization and further assist the switching in an ultrafast picosecond scale, a strain pulse is applied to the system at three H_{ext} values near the resonance state, as depicted in Figs. 4d-4f. When the strain pulse is on, the system gets excited rapidly to an enhanced large angle precession with a rise time of ~ 100 ps. When the strain pulse is off, the system at all three H_{ext} values shows relaxation behaviour and the magnetization is aligned with H_{ext} . This large angle precession caused by the resonance between ASWs and spin precession is maintained steadily for non-decaying strain amplitude. In addition, as the spin dynamics is a nonlinear system, the resonance can happen in a wide field range of several kOe: the required H_{ext} to cause resonance can deviate from H_{ext} that makes the spin precession frequency exactly equal to the strain frequency (Fig. 4c). For example, an external magnetic field of $H_{\text{ext}} = 21$ kOe has the maximum precession amplitude, while fields of $H_{\text{ext}} = 18$ kOe or 24 kOe can also excite resonance behavior with relatively smaller precession amplitudes. It can also be seen that the precession amplitudes with 0.1% or 0.2% strain yield similar values. The

magnetic resonance with $H_{\text{ext}} = 21$ kOe is enhanced when the strain increases from 0.1% to 0.5% (see Supplementary Fig. 12).

Discussion

We experimentally detected the ASWs with the response time down to the order of 10 picoseconds in perpendicular magnetic [Co/Pd]_n multilayers *via* a femtosecond laser pulse excitation. Through direct measurements of coherent phonon and magnetization, we observed a 60-GHz magnetic resonance when the frequencies of ASWs and spin precession approach each other. We developed a theoretical model and revealed the physical mechanism of magnetic resonance from the strain-spin interaction from an energy viewpoint. We have shown enhanced energy efficiency by manipulating the spins using the strain. With the same strain profile, a larger amplitude of oscillation is achieved in a perpendicular magnetic material, compared to that in an in-plane magnetic material. This shows that strain-assisted switching is more efficient in a perpendicular material. These results could pave a pathway to manipulate the magnetization precession and/or switch the magnetization at an extremely high frequency through strain-spin coupling by optimizing the parameters of multilayer materials.

Methods

Sample preparation and characterization. All samples with the stack of $[\text{Co}(x)/\text{Pd}(y)]_n/\text{Co}(x)/\text{Ta}(3)$ ($x = 0.30\sim 0.70$ nm; $y = 0.70\sim 1.80$ nm), from the bottom to top, are deposited on $\text{Si}/\text{SiO}_2(300$ nm) substrate at room temperature using a six-target Shamrock magnetron sputtering system with the ultra-high vacuum (base pressure $< 5.0 \times 10^{-8}$ Torr). The $[\text{Co}(0.8$ nm)/ $\text{Pd}(1.8$ nm)]₁₁ multilayer is seeded with $\text{Ta}(5$ nm)/ $\text{Pd}(5$ nm) bilayer, the others are seeded with $\text{Ta}(3$ nm)/ $\text{Pd}(3$ nm) bilayer. All layers are sputtered with D.C. power sources and element targets under an Ar working pressure of 2.0 mTorr. The magnetic properties of all samples are characterized using a Physical Property Measurement System (PPMS) with the Vibrating Sample Magnetometer (VSM) module.

TR-MOKE and TDTR measurement. Both TDTR and TR-MOKE methods are based on the ultrafast pump-probe technique. In this technique, pump pulses are utilized to excite the sample to a higher energy level followed by a recovery process, while probe pulses detect this change as a function of time delay. Other methods can be used to excite the magnetization⁵⁰. A mode-locked Ti:Sapphire laser with a pulse duration of ~ 100 fs and a center wavelength of 783 nm at a repetition rate of 80 MHz is used for TDTR and TR-MOKE measurements. A $10\times$ objective lens is used to produce a $1/e^2$ spot radius of $w_0 = 6$ μm for both pump and probe beams. In addition, an external magnetic field of up to 29 kOe (at $\theta_H = 80^\circ$ as defined in Fig. 1) is applied in both TR-MOKE and TDTR measurements. To identify the angular dependence of the magnetization oscillation, simulations are conducted where the field angle is tuned in a wider range from 50° to 90° , as shown in Supplementary Fig. 10. We find that the resonant precessional frequency depends on the angle of the external field. For our measurement setup, the field angle is limited to $80^\circ \leq \theta_H \leq 90^\circ$ to achieve sufficiently high fields and to ensure a clear optical path for the laser beam. Therefore, we set θ_H to be 80° for all measurements of $[\text{Co}/\text{Pd}]_n$ samples, in order to achieve the highest precessional frequency with the smallest field and meanwhile to maximize the TR-MOKE signals (see Supplementary Note 5).

Micromagnetic simulation. In order to simulate the coupling between acoustic strain wave and spin precession in the [Co(0.8 nm)/Pd(1.5 nm)]₁₁ multilayer oriented in <111>, we introduce a magnetostrictive energy term as a source of the ASWs in the free energy density for the [Co/Pd]_n multilayer systems. Through the transformation between the film coordinate in which the z axis is the [111] crystallographic orientation and the crystallographic Cartesian coordinate in which the z' axis is [001] crystallographic orientation, the magnetostriction energy is simplified as a temporal strain effective perpendicular anisotropy (see Supplementary Note 6)

$$F_{me}(\mathbf{r}, t) = \frac{3}{4} b_2 \eta(t) m_z(\mathbf{r}, t) \quad (2)$$

where b_2 is the magnetostriction coefficient⁵¹ and the value is 26×10^7 erg/cm³, $\eta(t)$ is amplitude of the strain tensor that is spatially uniform and varying in time. We use a sinusoid wave of $\eta(t)$ that its frequency is 60 GHz, provided by the TDTR experimental data. Secondly, we insert this term into the free energy density $F(\mathbf{r}, t)$ and extract the effective field for the LLG equation, to describe the magnetization dynamics driven by the system energy with magnetostrictive energy included (see Supplementary Note 6)

$$\mathbf{H}_{\text{eff}}(\mathbf{r}, t) = -\frac{\partial F(\mathbf{r}, t)}{\partial \mathbf{M}(\mathbf{r}, t)} \quad (3)$$

$$\frac{d\mathbf{M}(\mathbf{r}, t)}{dt} = -\frac{\gamma}{1+\alpha^2} \left[\mathbf{M} \times \mathbf{H}_{\text{eff}} + \frac{\alpha}{M_s} \mathbf{M} \times (\mathbf{M} \times \mathbf{H}_{\text{eff}}) \right] \quad (4)$$

where the first term describes the torque driving the precession of the magnetization vector around the effective time-dependent magnetic field $\mathbf{H}_{\text{eff}}(\mathbf{r}, t)$, the second term describes precession damping according to the phenomenological Gilbert damping parameter, and γ is the gyromagnetic ratio. The magnetization dynamics is started by providing an initial angle of magnetization that deviates from equilibrium. The amplitude of this angle ($\sim 1^\circ$) is one of the inputs to match a realistic angle from TR-MOKE measurements (as discussed in Supplementary Note 4).

Thirdly, we interpret analytically the time evolution of the total magnetization $\langle \mathbf{M}(\mathbf{r}, t) \rangle$ averaging in space, in analogy with a driven oscillator^{52,53}. With the first order approximation, the out-of-plane component of the magnetization is simplified as

$$\begin{aligned} & \frac{d^2 m_{y'}}{dt^2} + \gamma^2 (H_{\text{ext}} + H_{k0} \sin^2 \theta'_H) (H_{\text{ext}} - H_{k0} \cos(2\theta'_H)) m_{y'} \\ & + \alpha \gamma (2H_{\text{ext}} + H_{k0} \sin^2 \theta'_H - H_{k0} \cos(2\theta'_H)) \frac{dm_{y'}}{dt} \\ & = -\gamma^2 (H_{\text{ext}} + 2H_{k0} \sin^2 \theta'_H) \frac{\sin(2\theta'_H)}{2} \delta H_k \cos(\omega t) \end{aligned} \quad (5)$$

where the $m_{y'}$ is the out-of-plane component, H_{ext} is the external magnetic field, H_{k0} is the effective perpendicular anisotropy field, δH_k is the effective strain perpendicular anisotropy field and $\theta'_H = \frac{\pi}{2} - \theta_H$ (where θ_H is the external magnetic field). From Eq. (5), we can obtain the intrinsic frequency, the energy dissipation and the driving field. (see Supplementary Note 6D)

Data availability. The data supporting the plots within this paper and other findings of this study are available from the corresponding author upon reasonable request.

References

1. Kirilyuk, A., Kimel, A. V. and Rasing, T. Ultrafast optical manipulation of magnetic order. *Rev. Mod. Phys.* 82, 2731(2010).
2. Li, T. et al., Femtosecond switching of magnetism via strongly correlated spin-charge quantum excitations. *Nature* 496, 69–73 (2013).
3. Stupakiewicz, A. et al., Ultrafast nonthermal photo-magnetic recording in a transparent medium. *Nature* 542, 71–74 (2017).
4. Uchida, K. et al., Long-range spin Seebeck effect and acoustic spin pumping, *Nat. Mater.* 10, 737-741 (2011).
5. Temnov, V. V. Ultrafast acousto-magneto-plasmonics. *Nat. Photonics.* 6, 728-736 (2012).
6. Mentink, J. H. et al., Ultrafast spin dynamics in multisublattice magnets. *Phys. Rev. Lett.* 108, 057202 (2012).
7. Shen, K. and Bauer, G. E. W. Laser-induced spatiotemporal dynamics of magnetic films. *Phys. Rev. Lett.* 115, 197201 (2015).
8. Bonetti, S. et al., THz-driven ultrafast spin-lattice scattering in amorphous metallic ferromagnets. *Phys. Rev. Lett.* 117, 087205 (2016).
9. Thielemann-Kühn, N. et al., Ultrafast and energy-efficient quenching of spin order: Antiferromagnetism beats ferromagnetism. *Phys. Rev. Lett.* 119, 197202 (2017).
10. Man, H. et al., Direct observation of magnon-phonon coupling in yttrium iron garnet. *Phys. Rev. B* 96, 100406(R) (2017).
11. Holanda, J. et al., Detecting the phonon spin in magnon-phonon conversion experiments. *Nat. Phys.* 14, 500-506 (2018).
12. Vodungbo, B. et al., Laser-induced ultrafast demagnetization in the presence of a nanoscale magnetic domain network. *Nat. Commun.* 3, 999 (2012).
13. Kovalenko, O. et al. New concept for magnetization switching by ultrafast acoustic pulses. *Phys. Rev. Lett.* 110, 266602 (2013).
14. Graves, C. E. et al., Nanoscale spin reversal by non-local angular momentum transfer following ultrafast laser excitation in ferrimagnetic GdFeCo. *Nat. Mater.* 12, 293–298 (2013).
15. Wohlhüter, P. et al., Nanoscale switch for vortex polarization mediated by Bloch core formation in magnetic hybrid systems. *Nat. Commun.* 6, 7836 (2015).
16. Yang, Y. et al., Ultrafast magnetization reversal by picosecond electrical pulses. *Sci. Adv.* 3, e1603117 (2017).
17. Roy, K. et al., Hybrid spintronics and straintronics: A magnetic technology for ultra-low energy computing and signal processing. *Appl. Phys. Lett.* 99, 063108 (2011).

18. Lei, N. et al. Strain-controlled magnetic domain wall propagation in hybrid piezoelectric/ferromagnetic structures. *Nat. Commun.* 4, 1378 (2013).
19. Ranieri, E. D. et al. Piezoelectric control of the mobility of a domain wall driven by adiabatic and non-adiabatic torques. *Nat. Mater.* 12, 808-814 (2013).
20. Zhao, Z. et al. Giant voltage manipulation of MgO-based magnetic tunnel junctions via localized anisotropic strain: A potential pathway to ultra-energy-efficient memory technology. *Appl. Phys. Lett.* 109, 092403 (2016).
21. Beaurepaire, E. et al., Ultrafast spin dynamics in ferromagnetic Nickel. *Phys. Rev. Lett.* 76, 4250 (1996).
22. Malinowski, G. et al., Control of speed and efficiency of ultrafast demagnetization by direct transfer of spin angular momentum. *Nat. Phys.* 4, 855-858 (2008).
23. Bigot, J.-Y., Vomir M. and Beaurepaire. E. Coherent ultrafast magnetism induced by femtosecond laser pulses. *Nat. Phys.* 5, 515-520 (2009).
24. Zhang, G. P. et al., Paradigm of the time-resolved magneto-optical Kerr effect for femtosecond magnetism. *Nat. Phys.* 5, 499-502 (2009).
25. Müller, G. M. et al., Spin polarization in half-metals probed by femtosecond spin excitation. *Nat. Mater.* 8, 56-61 (2009).
26. Koopmans, B. et al., Explaining the paradoxical diversity of ultrafast laser-induced demagnetization. *Nat. Mater.* 9, 259-265 (2010).
27. Eschenlohr, A. et al., Ultrafast spin transport as key to femtosecond demagnetization. *Nat. Mater.* 12, 332-336 (2013).
28. Scherbakov, A. V. et al., Coherent magnetization precession in ferromagnetic (Ga,Mn)As induced by picosecond acoustic pulses. *Phys. Rev. Lett.* 105, 117204 (2010).
29. Thevenard, L. et al., Effect of picosecond strain pulses on thin layers of the ferromagnetic semiconductor (Ga,Mn)(As,P). *Phys. Rev. B* 82, 104422 (2010).
30. Kim, J.-W., Vomir, M. and Bigot. J.-Y. Ultrafast magnetoacoustics in Nickel films. *Phys. Rev. Lett.* 109, 166601 (2012).
31. Bombeck, M. et al., Excitation of spin waves in ferromagnetic (Ga,Mn)As layers by picosecond strain pulses. *Phys. Rev. B* 85, 195324 (2012).
32. J. V. Jäger, et al., Picosecond inverse magnetostriction in gallenol thin films. *Appl. Phys. Lett.* 103, 032409 (2013).
33. Bombeck, M. et al., Magnetization precession induced by quasitransverse picosecond strain pulses in (311) ferromagnetic (Ga,Mn)As. *Phys. Rev. B* 87, 060302(R) (2013).
34. Thevenard, L. et al., Surface-acoustic-wave-driven ferromagnetic resonance in (Ga,Mn)(As,P) epilayers. *Phys. Rev. B* 90, 094401 (2014).

35. Jäger, J. V. et al., Resonant driving of magnetization precession in a ferromagnetic layer by coherent monochromatic phonons. *Phys. Rev. B* 92, 020404(R) (2015).
36. Deb, M. et al., Picosecond acoustic-excitation-driven ultrafast magnetization dynamics in dielectric Bi-substituted yttrium iron garnet. *Phys. Rev. B* 98, 174407 (2018).
37. Jamali, M. et al., Spin-orbit torques in Co/Pd multilayer nanowires, *Phys. Rev. Lett.* 111, 246602 (2013).
38. Pal, S. et al., Optically induced spin wave dynamics in [Co/Pd]₈ antidot lattices with perpendicular magnetic anisotropy. *Appl. Phys. Lett.* 105, 162408 (2014).
39. Pal, S. et al., Ultrafast dynamics and THz oscillation in [Co/Pd]₈ multilayers. *Solid State Commun.* 221, 50-54 (2015).
40. Gilbert, D. A. et al., Realization of ground-state artificial skyrmion lattices at room temperature. *Nat. Commun.* 6, 8462 (2015).
41. Chesnel, K. et al., Shaping nanoscale magnetic domain memory in exchange-coupled ferromagnets by field cooling. *Nat. Commun.* 7, 11648 (2016).
42. Hashimoto, S., Ochiai, Y. and Aso, K. Perpendicular magnetic anisotropy and magnetostriction of sputtered Co/Pd and Co/Pt multilayered films. *J. Appl. Phys.* 66, 4909 (1989).
43. Schelp, L. F. et al., Magnetostriction of Co/Pd multilayers. *J. Magn. Magn. Mater.* 139, 59-64 (1995).
44. Zhu, J. et al., The ultrafast laser pump-probe technique for thermal characterization of materials with micro/nanostructures. *Nanoscale Microscale Thermophys. Eng.* 21, 177-198 (2017).
45. O'Hara, K. E., Hu, X. and Cahill, D. G. Characterization of nanostructured metal films by picosecond acoustics and interferometry, *J. Appl. Phys.* 90, 4852 (2001).
46. Mizukami, S. et al., Gilbert damping for various Ni₈₀Fe₂₀ thin films investigated using all-optical pump-probe detection and ferromagnetic resonance. *Appl. Phys. Express* 1, 121301(2008).
47. Barman, A. et al., Size dependent damping in picosecond dynamics of single nanomagnets. *Appl. Phys. Lett.* 90, 202504 (2007);
48. Lattery, D. M. et al., Quantitative analysis and optimization of magnetization precession initiated by ultrafast optical pulses. *Appl. Phys. Lett.* 113, 162405 (2018).
49. Lattery, D. M. et al., Low Gilbert damping constant in perpendicularly magnetized W/CoFeB/MgO films with high thermal stability. *Sci. Rep.* 8, 13395 (2018).
50. Kuszewski, P. et al., Optical probing of rayleigh wave driven magnetoacoustic resonance. *Phys. Rev. Applied* 10, 034036 (2018).

51. O'Handley, R. Modern Magnetic Materials. p414-415 (John Wiley & Sons, Inc., 2000).
52. Janušonis, J. et al., Ultrafast magnetoelastic probing of surface acoustic transients. Phys. Rev. B 94, 024415 (2016).
53. Chang, C. L. et al., Parametric frequency mixing in a magnetoelastically driven linear ferromagnetic-resonance oscillator. Phys. Rev. B 95, 060409(R) (2017).

Acknowledgements

This work was supported by C-SPIN, one of six centers of STARnet, a Semiconductor Research Corporation program, sponsored by MARCO and DARPA. We would like to thank Prof. Paul Crowell from University of Minnesota for valuable discussions and suggestions.

Author contributions

D.L.Z., J.Z., T.Q., R.H.V, X.W., and J.P.W. conceived the research. D.L.Z. designed and prepared all of the samples and carried out all magnetic measurements. J.Z. and D.M.L. designed and carried out the TDTR and TR-MOKE measurements and fitted the data. D.L.Z. and J.Z. introduced the initial experimental results including magnetic properties and TDTR and TR-MOKE data on this topic to T.Q. and suggested the need for theoretical analysis. T.Q. carried out the theoretical prediction, analytical derivation, and micromagnetic simulation that inspired the experimental results of the resonance. D.L.Z and J.Z participated in the discussion of the theory and micromagnetic simulation. D.L.Z., J.Z., and T.Q. prepared the figures and drafted the manuscript. J.P.W., X.W., and R.H.V. coordinated the project. All the authors discussed the results and commented on the manuscript.

Additional information

Supplementary information is available in the online version of the paper. Reprints and permissions information is available online at www.nature.com/reprints. Publisher's note: Springer Nature remains neutral with regard to jurisdictional claims in published maps and institutional affiliations. Correspondence and requests for materials should be addressed to J.P.W., X.W and R.V.

Competing financial interests

The authors declare no competing financial interests.

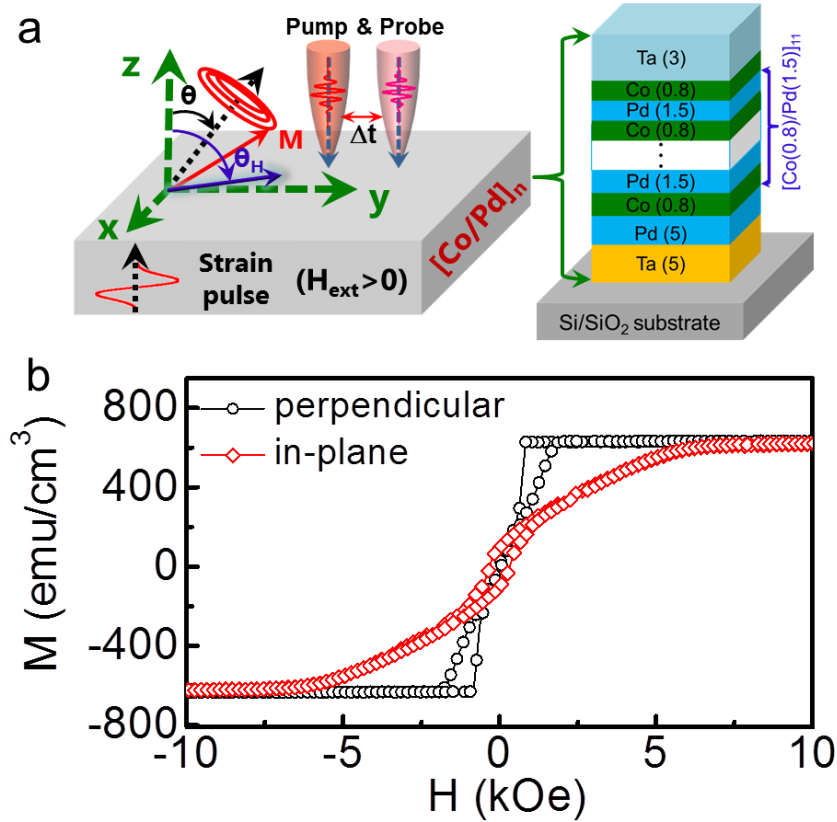


Figure 1 | Measurement protocol. **a**, Illustration of the ultrafast time-resolved magneto-optical Kerr effect (TR-MOKE) measurements (left) on the $[\text{Co/Pd}]_n$ multilayer with numbers in parentheses denoting layer thicknesses in nanometres (right). In TR-MOKE measurement, in the absence of an external magnetic field H_{ext} , the magnetostrictive effect can be measured, in which the acoustic strain wave induces the magnetization oscillation. The magnetization of $[\text{Co/Pd}]_n$ multilayer is tilted to the angle (θ) when $H_{\text{ext}} > 0$ is applied with the angle ($\theta_H = 80^\circ$). The TR-MOKE signals will include the signal from spin precession and acoustic strain wave. By fitting the data, we can separate them and identify their coupling. The figure in the right plane of the top shows the $[\text{Co/Pd}]_n$ multilayered structure used in our work. **b**, The magnetic hysteresis (M-H) loops of the $[\text{Co}(0.8 \text{ nm})/\text{Pd}(1.5 \text{ nm})]_{11}$ multilayer with a magnetic anisotropy field $H_{k,\text{eff}} \sim 6.5 \text{ kOe}$.

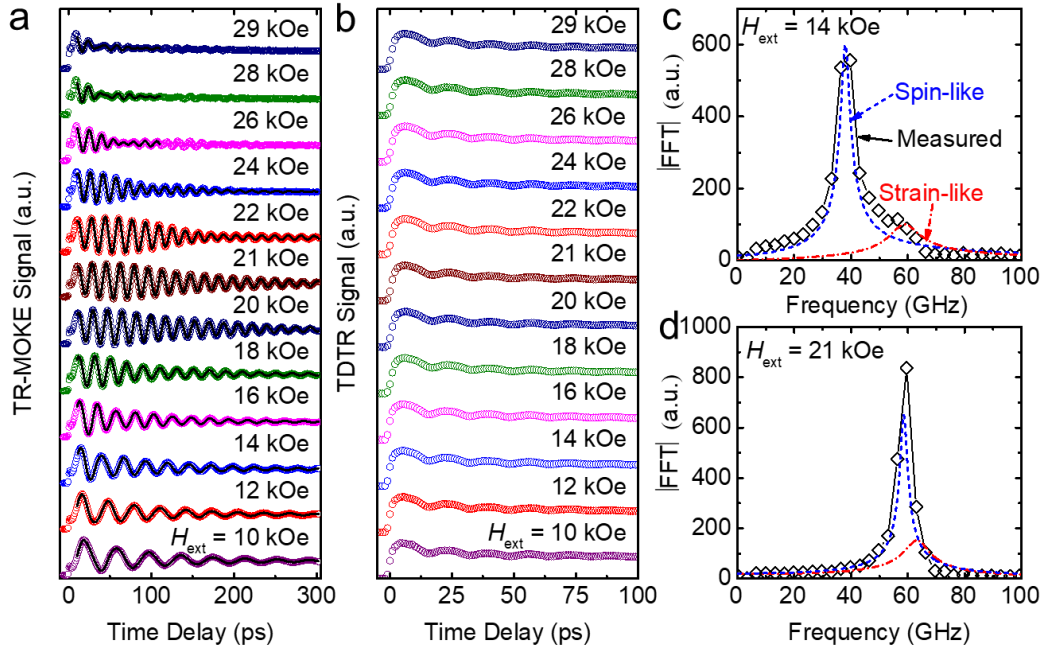


Figure 2 | Ultrafast measurement results. **a**, the experimental and fitting TR-MOKE signals and **b**, the experimental TDTR signals as a function of H_{ext} (10 to 29 kOe). It is clearly seen that TDTR signals do not change in the whole region of H_{ext} while TR-MOKE signals show different oscillation patterns with external fields. For $H_{\text{ext}} < 16$ kOe or > 25 kOe, magnetization precession presents the damped oscillation, while for $16 \text{ kOe} < H_{\text{ext}} < 25 \text{ kOe}$, magnetization shows the resonance phenomenon. **c,d**, Fourier transform of the TR-MOKE signal with $H_{\text{ext}} = 14$ kOe and 21 kOe, respectively, from which two peaks (spin-like and strain-like) can be found. For $H_{\text{ext}} = 14$ kOe, the two peaks are separate, however, the two peaks are overlapping when $H_{\text{ext}} = 21$ kOe.

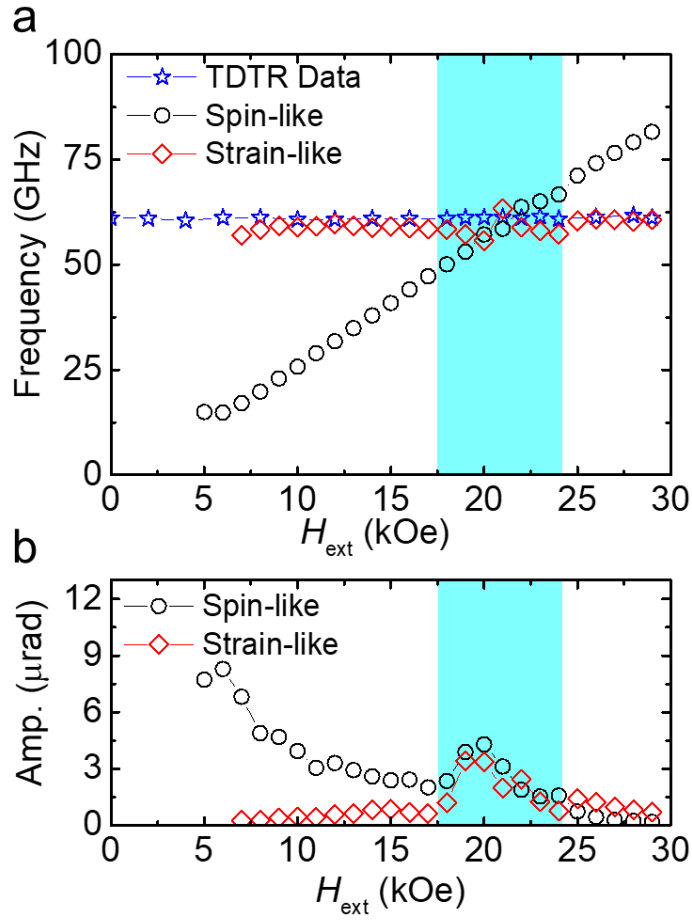


Figure 3 | Ultra-high frequency magnetic resonance. **a**, The frequency of the [Co(0.8 nm)/Pd(1.5 nm)]₁₁ multilayer as a function of H_{ext} . Two frequencies of spin precession (spin-like mode, open black circles and strain-like mode, open red diamonds) are derived by fitting the experimental data of TR-MOKE. The figure also includes the frequency of ASWs measured from the TDTR method. It is clearly found that the ASW frequencies from TDTR and strain-like mode from TR-MOKE are nearly identical and independent of the external fields. While the frequency of spin precession increases linearly with the increase of H_{ext} . The resonance peak frequency occurs at an external field of ~ 21 kOe. **b**, The individual M_z amplitudes of spin-like and strain-like modes as a function of H_{ext} for the [Co(0.8 nm)/Pd(1.5 nm)]₁₁ multilayer. There exists an apparent amplification of both modes due to the coupling between spin precession and ASWs near the resonance frequency (the region highlighted in blue).

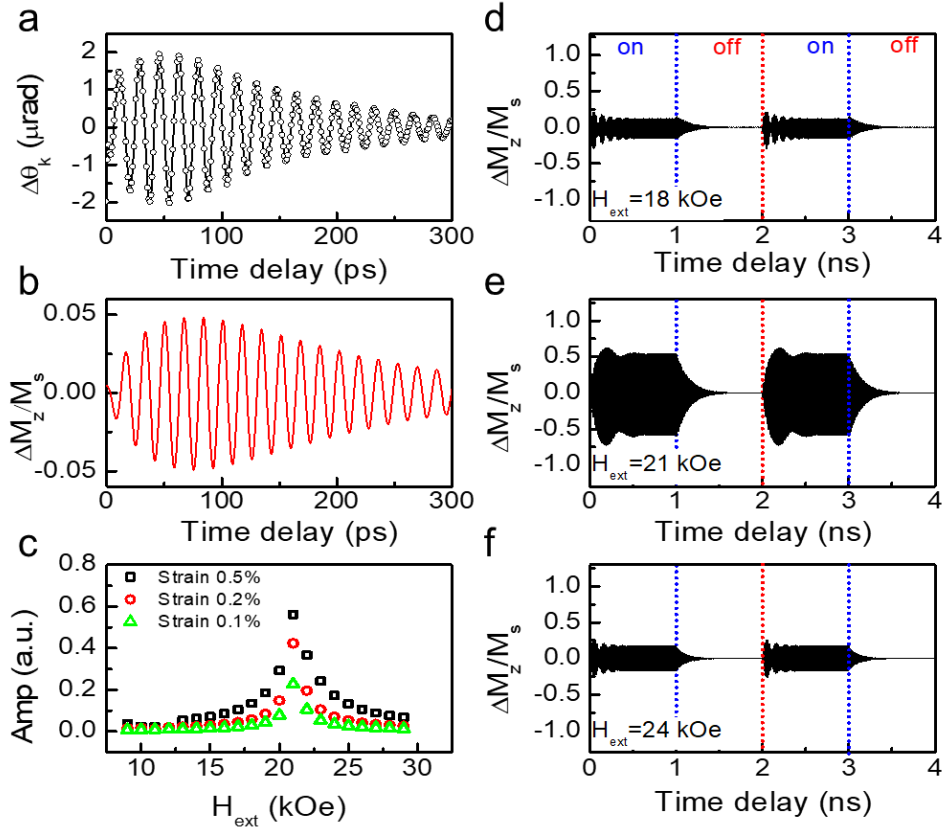


Figure 4 | Time-dependent magnetization dynamics. **a,b**, The experimental and simulated TR-MOKE signal of the $[\text{Co}(0.8 \text{ nm})/\text{Pd}(1.5 \text{ nm})]_{11}$ multilayer with $H_{\text{ext}} = 21 \text{ kOe}$, respectively. **c**, The oscillation amplitude versus H_{ext} for different strain amplitudes (0.1%, 0.2% and 0.5%). The time evolution of the out-of-plane magnetization vs. the time delay when a square strain pulse is applied. The pulse amplitude is 0.5%, the time period is 2.0 ns and the pulse length is 1.0 ns. **d-f**, The simulated spin precession coupled with a 0.5% strain pulse under H_{ext} of 18 kOe, 21 kOe and 24 kOe, respectively. When the strain pulse is on, the system gets excited rapidly to an enhanced large angle precession with a rise time of $\sim 100 \text{ ps}$ under $H_{\text{ext}} = 21 \text{ kOe}$ not 18 kOe and 24 kOe. When the strain pulse is off, the system at all three H_{ext} values shows relaxation behavior.